Geomorphology 185 (2013) 110–122

Contents lists available at SciVerse ScienceDirect

Geomorphology

journal homepage: www.elsevier.com/locate/geomorph

Photogrammetry and laser scanning for analyzing slope stability and rock fall runout along the Domodossola–Iselle railway, the Italian Alps

R. Salvini *, M. Francioni, S. Riccucci, F. Bonciani, I. Callegari

Earth Sciences Department and Centre of Geotechnologies, University of Siena, Via Vetri Vecchi 34, 52027 San Giovanni Valdarno (AR), Italy

ARTICLE INFO

Article history:
Received 12 July 2011
Received in revised form 21 September 2012
Accepted 19 December 2012
Available online 2 January 2013

Keywords:
Rocky slope
Photogrammetry
Laser scanning
Stability analysis
Runout

ABSTRACT

In Italy, railways crossing the alpine valleys are a vital means of civil and commercial communications with the rest of Europe. The geomorphologic configuration and the climatic conditions, especially in winter and spring, can cause rock fall events resulting in railway service interruptions and damage to infrastructure and, in the worst case, to people. There were rock fall events at a slope adjacent to the Domodossola–Iselle railway, most recently in 2004.

This paper evaluates the stability of a mountain slope and maps rock fall hazards through the modeling of potential runout trajectories. Traditional geological, geomorphological and geo-engineering surveys were combined with data derived from digital terrestrial photogrammetry. Stereo photographic pairs of rocky outcrops in inaccessible areas were acquired from a helicopter. Data from photogrammetry, topographic measurements and laser scanning were then integrated to build a digital model of the slope, to characterize the rock mass and block geometry, and to define possible runout trajectories. The geomatic methods used have yielded oriented stereo-images, orthophotos and precise digital models of rocky wedges. Geometrical and structural characteristics of slopes, such as joint attitude, spacing and persistence, and block volumes, were also derived. The results were used together with a deterministic limit equilibrium method to evaluate slope stability. We assessed the probabilistic distribution of rock fall end points and kinetic energy along the rock falling paths and existing barriers, and created a hazard map based on the spatial distribution of trajectories, rock fall transit density and kinetic energy.

1. Introduction

The risk of rock falls along roads and railways is particularly high in alpine valleys in which structural and climatic factors favor the formation of rocky blocks on steep slopes. Recent incidents of slope instability along the Domodossola–Iselle railway (Verbano–Cusio–Ossola Province, VB, Italy), notably between the tunnels of San Giovanni (to the south, km 7 + 300) and Gabbio Mollo (to the north, km 7 + 800), led the Italian rail line maintenance and safety authority (*Rete Ferroviaria Italiana*, RFI) to carry out an in-depth study of rock stability. The presence of large angular boulders at the bottom of the valley implies that this area has experienced rock falls, leading to serious problems for the railway. In the 1980s, for example, a block crashed through the protective barriers and hit a train. In 2004, a wedge of rock crashed through the barriers and electric cables, breaking the track. Numerous protective barriers have been installed since the 1980s by the RFI and also *Azienda Nazionale Autonoma delle Strade* (ANAS), the Italian road maintenance authority, because the SS 33 Sempione Highway runs next to the railroad (Fig. 1).

In any in-depth study of geomorphologic processes acting on steep mountain slopes, it is necessary to consider geology, topography, climate and land use/cover (Whalley, 1984; Evans and Savigny, 1994; Matsuoka and Sakai, 1999; Montgomery and Brandon, 2002; Marquinez et al., 2003; Hyndman and Hyndman, 2008; Loye et al., 2008). Together, these factors induce rock fracturing, opening of joints, rainfall infiltration and subsequent pore pressure increase, freeze–thaw processes in mountainous regions, and chemical weathering (Lim et al., 2004). Once the rock has detached, land use/cover and slope geometry dictate its trajectory. Assessment of rock fall hazard is limited partly by the lack of detailed data on slope topography, rock fall source areas, rock block geometry, and rock fall paths including runout distance (Hutchinson, 1988; Evans and Hungr, 1993; Dorren, 2003). Moreover, the reliability of rock fall hazard estimates depends upon the quality and quantity of historical data (Hutchinson et al., 2006). Owing to the steepness of mountain slopes, conventional survey methods have limitations on the collection of the spatial datasets required for rock fall modeling.

In the present research, we used digital terrestrial photogrammetry (DTP) and terrestrial laser scanning (TLS) to study the stability of rocky slopes and rock fall hazards. In addition to geological information from the literature and new in-depth surveys, these geomatic technologies, which have become widespread in geological applications, have successfully provided accurate geometrical data regarding

* Corresponding author. Tel.: +39 0559119441; fax: +39 0559119439.
E-mail address: riccardo.salvini@unisi.it (R. Salvini).

0169-555X/$ – see front matter
http://dx.doi.org/10.1016/j.geomorph.2012.12.020

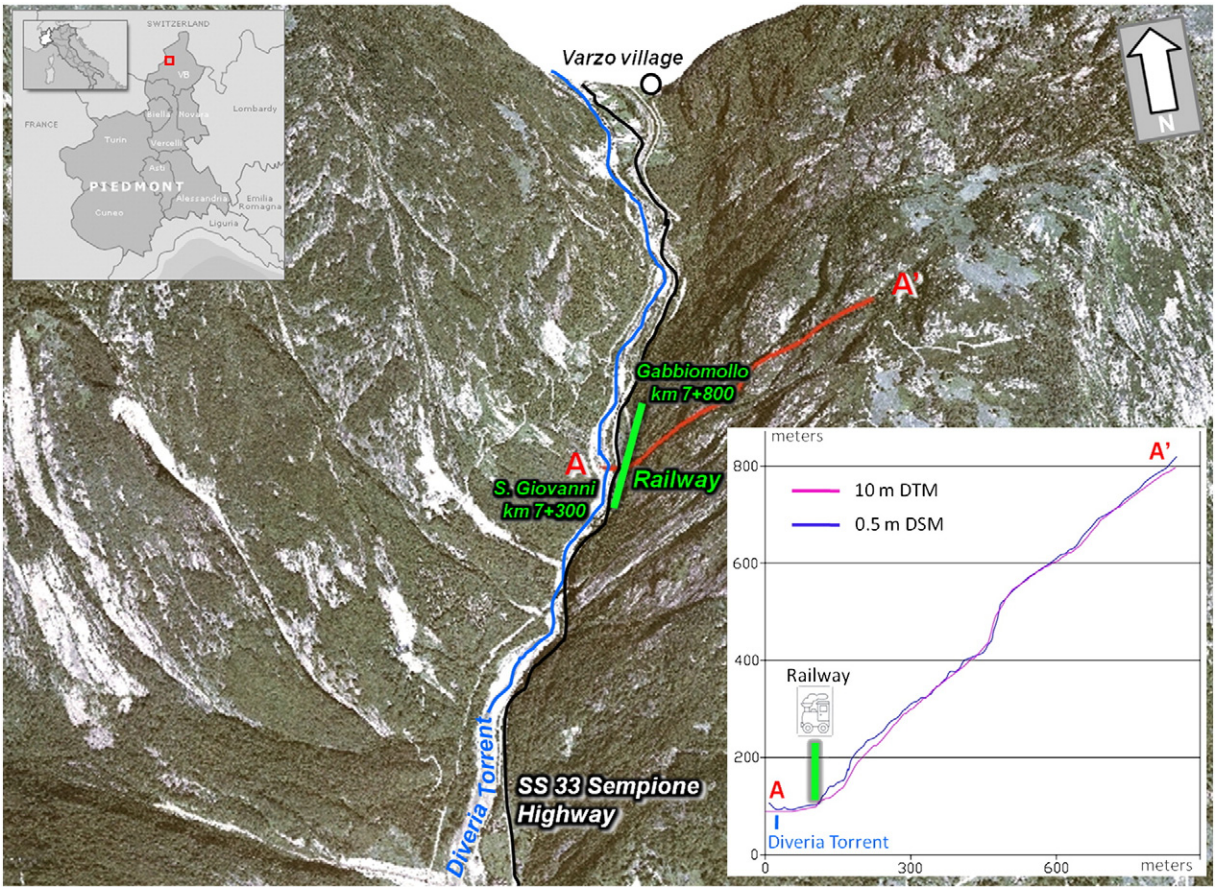

Fig. 1. Perspective view of the study area. Aerial orthophotos overlaid on the 10 m DTM from topographic maps. Cross sections (A–A′) are from the 0.5 m DSM and DTM. Inset map shows the location of the study area.

slopes, discontinuities and blocks even in unreachable areas. Today TLS is the best way to represent slope geometry (Feng and Röshoff, 2004a; Abellán et al., 2006; Yoon et al., 2006; Yohei et al., 2007; Runqiu and Xiujun, 2008; Armesto et al., 2009) and characterize rock mass (Feng and Röshoff, 2004b; Van Knapen and Slob, 2006; Ferrero et al., 2009; Fekete et al., 2010). DTP also provides information about the structural and geo-engineering setting of slopes. Joint systems can be studied over all parts of a slope, and the geometry of any visible potentially unstable wedges can be measured. DTP has already been used to characterize rocky masses (Wickens and Barton, 1971; Mosaad Allam, 1978; Zhang and Kulatilake, 2003; Di Crescenzo and Santo, 2007; Haneberg, 2008; Ferrero et al., 2009) and in monitoring slope stability (Takumi et al., 2000; Ohnishi et al., 2006). The altitude and complex morphology of alpine mountain slopes render them inaccessible for the collection of geometrical data on joints and rocky blocks along the whole versant. By mounting the photogrammetric equipment on a helicopter (Vallet et al., 2000; Copons and Vilaplana, 2008; Haarbrink and Eisenbeiss, 2008), photos can be taken from an optimal viewpoint and orthogonal to the slope, so that no areas fail to be covered.

Given the geometrical data from DTP and TLS, conventional methods of limit equilibrium can be applied so as to study slope stability in a deterministic way. To properly assess the rock fall processes, it is necessary to use topographic data with a resolution relevant to the scale of morphological features being examined (Glenn et al., 2006). DTP and TLS then represent a powerful tool not only for slope stability analysis, but also for rock fall runout (Kaab, 2000; Monnet et al., 2010). Detailed information about trajectories is based on a digital model of the slope, as well as land cover and block source points involving interpretation of the photographs. Rock falls can then be simulated. We analyze the end point of a rock fall block and the kinetic energy along the falling path via a 2D analysis, assuming that the fall follows the path of the steepest descent. This neglect of lateral momentum can lead to significant errors in assessing rock fall hazard (Crosta and Agliardi, 2004), and accurate estimation of rock fall hazard should be more complex (Acosta et al., 2003; Crosta and Agliardi, 2003). We modeled the spatial distribution of rock fall frequency, velocity and kinetic energy using the 'cone' method (Toppe, 1987; Jaboyedoff and Labiouse, 2003; Jaboyedoff et al., 2005). In this way the accuracy of analysis was improved, based on a 2.5D modeling approach. Because of the presence of protective barriers, several simulations were carried out, varying the maximum safe impact energy in terms of the barrier type, size and condition. To assess the hazard, the spatial distribution of rock fall frequency and energy was combined with historical data and a geomorphologic map.

2. Regional setting

The study area, 5 km downstream of Varzo Village (Fig. 1), is located in the Divedro Valley separating the Lepontine and Pennine Alps. The rocky front under study, located on the left bank of the Diveria Torrent, is 550 m wide and 650 m high, with an average slope of about 43° and some vertical escarpments that interrupt the general trend. The elevation of the crests ranges between 1380 and 1735 masl, and the riverbed is about 400 masl.

2.1. Geological setting

The European-vergent Alpine chain is divided into several tectonic systems, which are gathered in groups of nappes either with similar

kinematic histories or belonging to the same palaeogeographic tethydic Mesozoic basin. A complete geological section of the Alps, from the lower Sudalpine up to the Pennidic and Austroalpine nappes (CNR, 1990), outcrops in the VB Province. The study area includes parts of the tectonic system of the Pennidic Zone, divided into upper (or internal), middle and lower (or external) nappes. The lower Pennidic nappes are visible in the Ossola–Ticino tectonic window, including (from the top) the Monte Leone unit, the Lebendun sequence, the Antigorio nappe, and the upper part of the Verampio dome, which is the deepest visible alpine unit (Argand, 1911). The lower Pennidic nappes (Upper Paleozoic/Mesozoic) are composed of gneiss, granites and metamorphic sequences.

Only the Antigorio nappe was surveyed during the geologic fieldwork (Fig. 2); this is represented by orthogneiss that is characterized by centimetric and pluri-centimetric crystals of feldspar, black mica, and biotite (Hunziker, 1966; Joos, 1969; Bigioggero et al., 1977). Following Boriani (2000), we surveyed two different lithofacies. The first, outcropping in the lower-intermediate part of the slope, is characterized by a weakly visible and highly spaced schistosity with a massive structure. At the higher part of the slope the second facies of orthogneiss outcrops with the same mineralogical-petrographic composition, but with a more marked and thicker schistosity. The Antigorio nappe outcrops correspond to an area larger than the one under study (ARPA *Regione Piemonte*, 2008); this is because it is included within the recumbent structure, which involves the lower Pennidic nappes, with an SE dip direction of schistosity and a dip increasing from north to south. The Pennidic nappes are characterized by isoclinal folds (e.g. the Antigorio antiform in the study area), which are interpreted as post-nappe secondary structures. Associated mesoscale structures, present in the Europe-vergent Antigorio fold, are also visible on the wall of a quarry located near the study area.

In regard to post-collisional brittle structures, the area contains some visible faults with thick breccias that could act as the source of surface or of deep-seated gravitational slope deformations. Near Domodossola, 10 km south of Varzo Village, the Simplon regional tectonic lineament, which is a normal detachment low angle fault, causes regional unroofing of the Alpine structure, leading to the outcrop of the deepest units (Mantckelow, 1985) and separating the lower Pennidic nappes from the middle and upper units.

2.2. Geomorphological setting

The area is a typical alpine landscape with steep slopes interrupted by vertical escarpments that link the valley through ridges, with a relative height ranging from 600 to 1000 m. The flat and large Diveria riverbed has been produced by aggradations of glacial–fluvial sediments, as

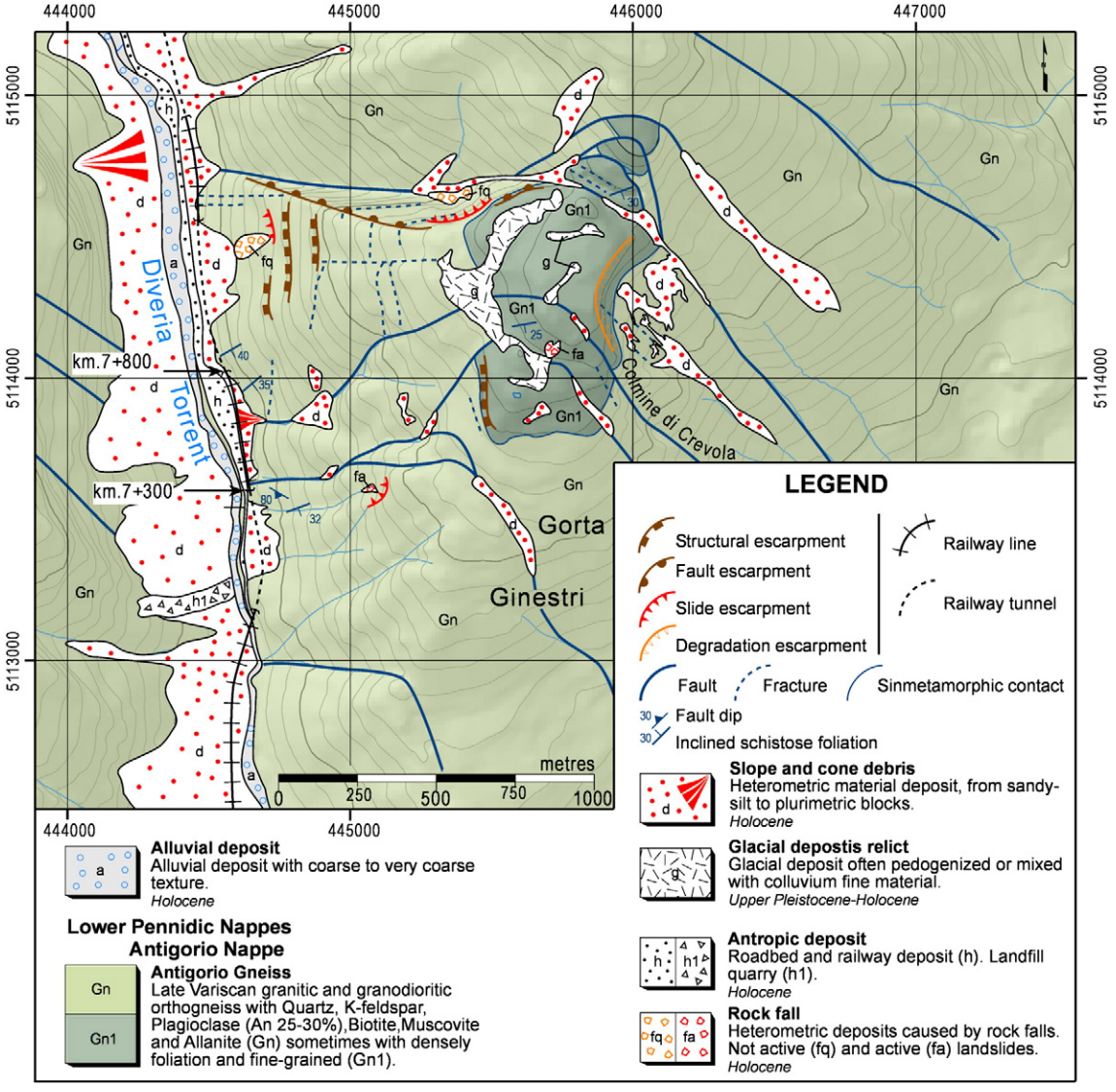

Fig. 2. Geological–geomorphological map (UTM projection, datum WGS84, zone 32 north).

indicated by large rounded boulders at the valley bottom; other highly angular blocks stem from falls from the surrounding rocky slopes.

The stream network is complex, and lower order streams flow into the Diveria as intense seasonal flash floods.

The Diveria runs along a typical glacial U-shaped valley with *roches moutonnée*, erratics, grooves and striated or polished rocks. Rock falls are generally caused by cryoclastic cycles, and large amounts of detrital deposit are found at foothills and valley bottoms. Such deposits are due to rock falls, as at km 7 + 550, where rocks that were recently fallen ended up on a detrital cone (Fig. 2). Rock blocks larger than 1 m^3 are common, and the most abundant fallen material has sizes of a few centimeters to half meter. Photointerpretation and geological surveys allowed us to identify faults of decametric length that also contribute to slope instability.

3. Material and methods

The flowchart in Fig. 3 sets out the methodology of this research.

3.1. Geo-engineering survey

Geo-engineering data were collected during fieldwork, for rock mass classification, slope stability assessment and hazard zoning. Specifically, we determined the rock mass rating (*RMR*; Bieniawski, 1989), integrated with the slope mass rating (*SMR*; Romana, 1985). To assess the results, we used the *Q* System classification (Barton et al., 1974).

3.2. Terrestrial laser scanning

In order to analyze slope stability, we extracted geometrical data from the high resolution digital surface model (DSM). A Riegel™ Z420i terrestrial laser scanner was used to acquire two 50% overlapping point clouds from two distinct positions, avoiding shadows as much as possible. The distance between the slope and the instrument ranged from 300 to 800 m and the spatial resolution of the point clouds was set to 5 cm for a 500 m distance, corresponding to a scanning angle of 0.006°. The two point clouds were stored and processed using the Leica™ Cyclone software.

Using a Leica™ TCRP 1203+R1000 total station, a topographic survey of cylindrical retroreflectors (height and diameter equal to 100 mm) was performed to refer the scans to the same coordinate system. Reflectors were located in reachable zones to provide an optimal spatial distribution with a distance from 20 to 70 m. To determine absolute coordinates for these targets, a differential GPS survey was performed with a Leica™ 1200 GPS receiver. The root mean square error (*RMSE*) of GPS measurement, corrected using the Leica ™ GeoOffice software based on contemporary data recorded by the Luino permanent station (Varese Province, VA, Italy), was 3 cm. Post-processing procedures to compute the ground coordinates of the reflectors were therefore able to integrate the two scan-worlds into a single system. To minimize co-registration errors, cloud constraints were created by adding custom targets on the slope represented by protection works, electric lines and train/road signs. Following this rough matching, an automated procedure using a point-to-surface "iterative closest point" algorithm (Besl and McKay, 1992) was used to minimize the co-registration errors. The residual of this procedure was assessed on the targets (4 mm) and on the slope (8 cm mean on planar faces where the scans overlap).

From processing of the cloud of points, the slope geometry was represented first by a triangulated irregular network (TIN), and was then converted to a grid format. In areas covered by vegetation and those where irregular slope geometry made laser pathway detection impossible, the cloud of points was treated by the stereorestitution of 3D features and by automatic filtering, to avoid errors arising from not-bare terrain points and the interpolation process. Fig. 1 shows the differences between the digital terrain model available from topographic maps (DTM, 10 m spatial resolution) and the created DSM (0.5 m spatial resolution). As the highly accurate DSM may improve the estimation of modeling parameters and reduce model structural errors for assessing rock fall hazards (Lan et al., 2010), we computed the differences in elevation between the DSM and the DTM, following Höhle and Höhle (2009).

3.3. Photogrammetric survey and spatial modeling

DTP was applied to the detailed photointerpretation of rocky blocks and joints in inaccessible zones. The photogrammetric equipment, hooked up to the lateral hamper of a helicopter, consisted of an aluminum frame supporting two Nikon™ D80 digital cameras (physical CCD frame size 2.36 × 1.58 cm, with 10.2 million effective pixels), and two GPS antennas at its extremities (5 m baseline). Nikon™ AF Nikkor 20 mm f/2.8 lenses were used, with a coverage angle of 70°. Horizontal and vertical fields of view varied with

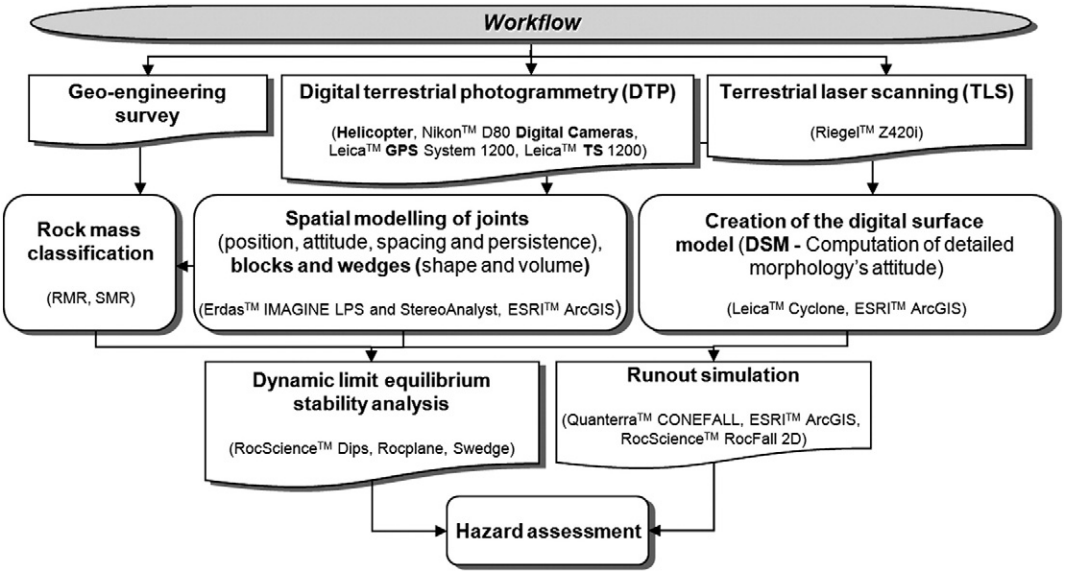

Fig. 3. Methodology of this research.

distance from an outcrop. We aimed to keep the scale of photographs within the same strip as constant as possible. Among different strips the *b*/*h* ratio (baseline/distance from the target) ranged from 0.05 to 0.1, corresponding to distances from the slope of 50 to 100 m. This variation was unavoidable in view of the extremely varied slope shape.

Image acquisition was controlled by a PC-driven radio system which guarantees simultaneity and setting of the shot angle in relation to the north. This function reduces difficulties, concerning the yaw angle, in maintaining the orthogonality of the system relative to the slope, thereby enhancing the orientation process and the integrity of individual 3D relative models. The procedure was managed using the Dragonfly software package (Menci Software™), while image quality was assessed in real-time using the Nikon™ Camera Control Pro software. In this way, while the helicopter was hovering in front of the slope, the cameras took simultaneous photos at various altitudes, and the GPS receivers recorded the perspective center positions of the cameras in order to determine the direction of the aluminum frame relative to the north. We undertook the geometric calibration of the entire system, including the relative position and attitude of the center of perspective of the cameras relative to GPS antennas, in our previous studies (Firpo et al., 2011; Salvini et al., 2011) by means of a detailed topographical survey of the equipment and dedicated flights.

Comprehensive photographic acquisition of the area, including a 30% sidelap, was achieved using eight vertical strips with about 10 stereopairs each. GPS receivers functioned in real time kinematic modality (RTK) with respect to a reference point near the railway line. The GPS post-processing, relative to the Luino permanent station, yielded the absolute position for each shot. Because of the lack of inertial data relative to pitch, roll and yaw angles, we based the external orientation of the stereoscopic models on a survey we made of 150 ground control points (GCPs) using the total station and differential GPS.

The *RMSE* value of the external orientation determined using the ERDAS™ IMAGINE LPS module varies among the eight different strips; the system was solved as separate strips rather than a single block, since the direction of acquisition of photos varied in order to maintain orthogonality to the slope. This capture mode gave a good stereoscopic view and accuracy of the resulting measures. Table 1 summarizes the results of the external orientation.

Geological features were reconstituted from the stereoscopic photographic views. Using the StereoAnalyst module of ERDAS™ IMAGINE, joint surfaces were represented by triangles, and their attitudes were calculated using techniques of spatial analysis. The geometry of blocks and of wedges was digitized as point features, whereas the persistence and spacing of fractures were measured as linear features. To check the accuracy of the stereorestituted elements, the attitude of large and well-defined planes in the stereoscopic model was compared with the TLS point cloud, which was not biased and not prone to manual errors. This is particularly important for inaccessible sites. Fig. 4 shows an example of eight rock surfaces related to five zones on the slope. For every surface, five planes were drawn and measured on the stereoscopic models and the TLS cloud of points. The stereographic projections and dip parameter values in Fig. 4 demonstrate the high accuracy of DTP, with mean values similar to those of TLS and differences smaller than 4° in dip direction and 8° in dip angle. This test demonstrates that DTP orientation and stereorestitution did not affect the measurements. The standard deviation of attitudes derived from DTP smaller than 10° also indicates the precision of this technique.

Using the stereorestituted 3D features and Rhinoceros™ SR3, wedges, joints and blocks were modeled so as to define closed spaces, from which their volumes and barycenters could be derived (Fig. 5). Thanks to the GPS survey, the coordinates of the barycenters were also known in the absolute coordinate system, and can be used as source points in rock fall analysis.

The photos were also orthorectified and mosaicked to aid the mapping of failures, land cover and artificial barriers (Fig. 6). The data from TLS, DTP and geo-engineering surveys were managed in a geographic information system (GIS).

3.4. Stability analysis

The analysis of rocky-block stability was made using conventional limit equilibrium methods and the Markland test (Markland, 1972). The softwares Rocplane 2.0 and Swedge 5.0 (Rocscience™) were used to simulate the sliding of blocks along planes and lines of intersection between joints. The physical–mechanical properties of the intact material and its discontinuities, necessary to calculate the shear strength, came from our fieldwork, while the geometrical setting of joints, volume of blocks and estimated joint normal stress were from DTP, and slope attitudes were from TLS. The empirical criterion of Barton and Bandis (1990) was applied to the safety factor (*SF*) calculation, and the coefficients deriving from fieldwork include the joint wall compressive strength (*JCS*; Deere and Miller, 1966), the joint roughness coefficient (*JRC*; Barton, 1973) and the basic friction angle (ϕ_b).

Stability analysis was carried out under both static and dynamic conditions, based on the percentage of water saturation in joints evaluated through a back analysis approach, starting from rock falls related to severe meteorological events (the analysis did not consider cryoclastic processes during winter months). The water percentage, necessary to bring *SF* below the critical value, was calculated. Local seismic acceleration was also considered, using the GeoStru PS software (GeoStru, 2008) to derive a dimensionless number that defines the seismic acceleration as a fraction of the acceleration due to gravity, the so-called "seismic coefficient" (0.056 in this study). A probability study on *SF* was performed to determine the effects of possible joint attitude changes ($\pm 5°$) on the stability analysis. The procedure was carried out following the *Norme Tecniche per le Costruzioni* (NTC) (M. LL. PP., 2008) and a *SF* limit of 1.3, based on the Italian Ministerial Decree 11.03.1988 (M. LL. PP., 1988).

3.5. Runout simulation

The processing of the DSM allowed us to calculate the probable trajectories of rock fall using the ArcHydro module of ESRI™ ArcMap

Table 1
Results of external orientation of photogrammetric strips.

Strip n.	Direction of acquisition (degree north)	Mean scale denominator	Pixel resolution on the ground	*RMSE* (image unit — pixel)	*RMSE* (ground unit — meter)
Strip-1	75	277	0.02	0.97	0.03
Strip-2	57	217	0.02	1.20	0.02
Strip-3	73	351	0.03	2.20	0.07
Strip-4	74	308	0.03	1.13	0.03
Strip-5	74	404	0.03	1.60	0.05
Strip-6	77	325	0.03	0.78	0.02
Strip-7	81	290	0.02	1.77	0.04
Strip-8	80	329	0.03	1.53	0.04

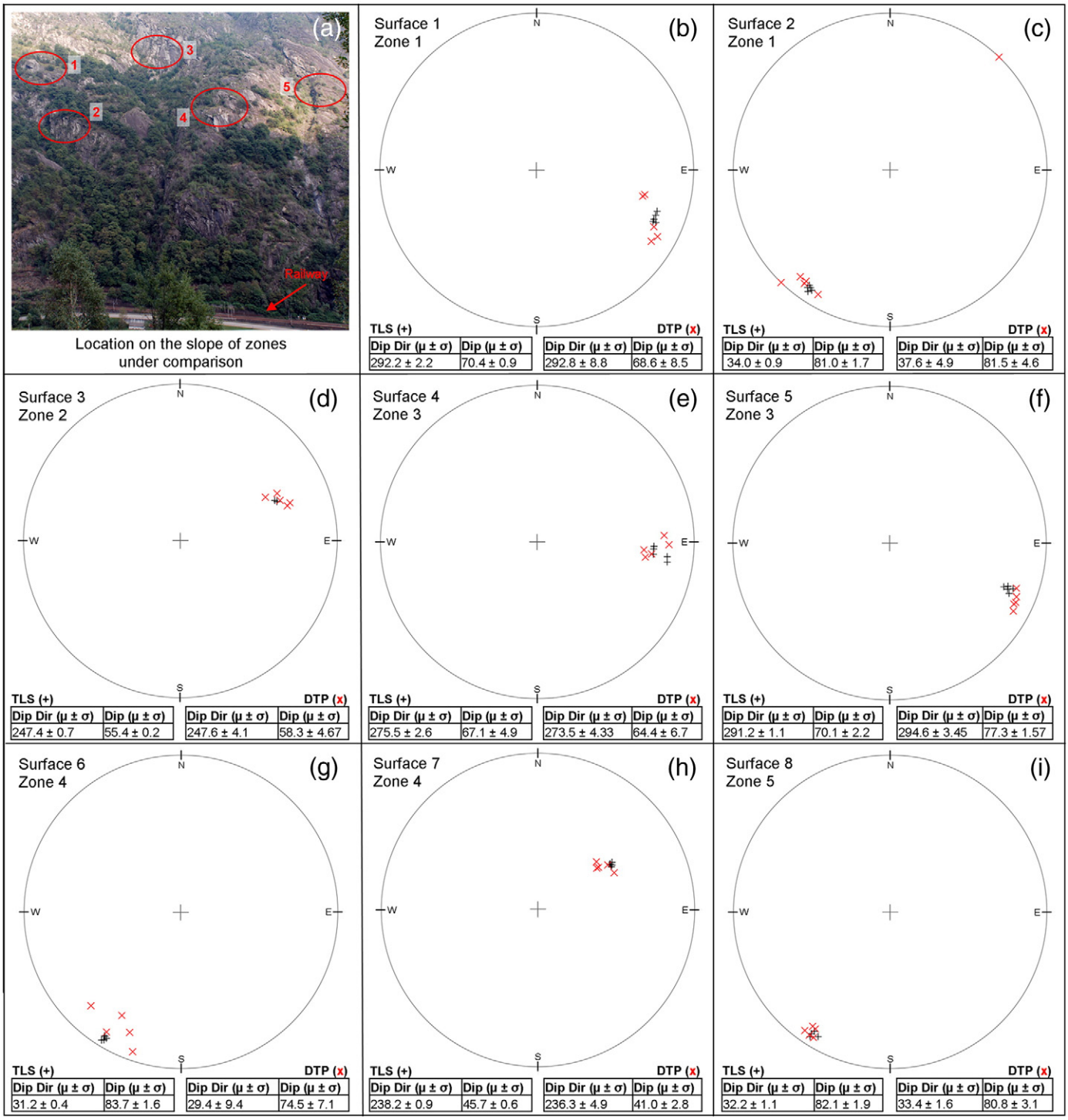

Fig. 4. Accuracy assessment of dip and dip direction values for rocky surfaces measured on the stereoscopic model and TLS point cloud. (a) Location on the slope of zones under comparison. (b–i) Stereographic projections using the Wulff equal-angle method, showing the spatial distribution of the surface attitude; tables state the mean (μ) and standard deviation (σ) of measures.

under the assumption that rock falls follow the path of the steepest descent. The morphological profile of rock fall paths was obtained by the interpolation of 3D points derived from a procedure developed in Esri™ Arcinfo Workstation, integrated with the Easy Profiler tool of Esri™ ArcMap. The weight of blocks, land cover (bedrock, debris, shrubbery and arborous vegetation) and the distribution of protective barriers classified basing on their type (rigid, elastic or semi-elastic), state of preservation and height (Fig. 6), were used as input data to the RocFall 4.0 software (Rocscience™), so as to analyze the runout. Local conditions were accounted for via a statistical approach, using the standard deviation of the coefficients of normal and tangential restitution to obtain probabilistic results. Since RocFall does not consider block fragmentation while falling, the coefficients of normal and tangential restitution were calibrated based on the size of collapsed wedges. The downslope dispersion area was then estimated using the Quanterra™ Conefall software, which is based on different principles of rock fall simulation: a block can accelerate down a steep slope but decelerates on a slope gentler than a certain angle (Heim, 1932).

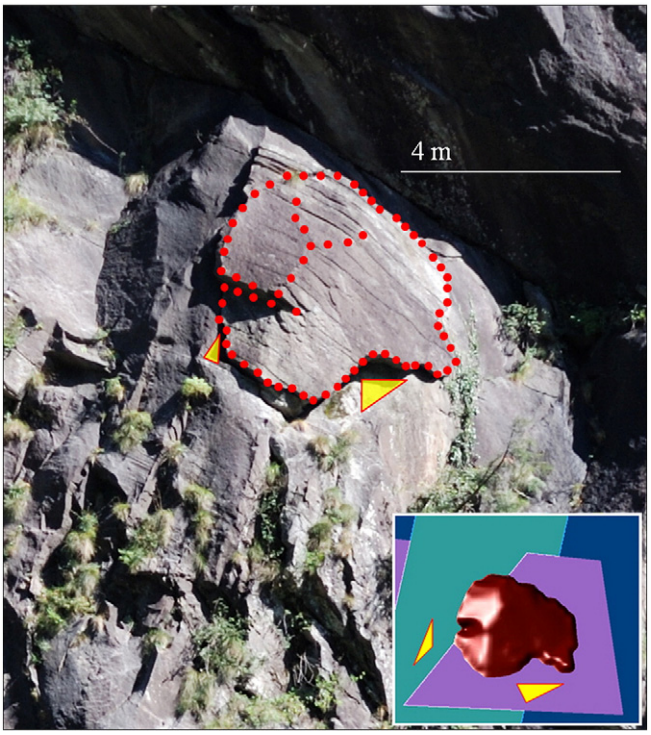

Fig. 5. Photograph showing an example of block and joints restitution by means of points and triangles; in the lower right the related 3D modeling is shown.

During rock falls, gravitational potential energy is converted into kinetic energy. The line connecting the source and end of rock fall is called the "energy line", and its gradient is called the "energy line angle" (43.3° in this study). A block may propagate laterally within a cone-shaped slope having the energy line angle as its axis and vertex at the source point. According to the principle of gravitational potential energy at any point of the propagation zone, the vertical component of the energy line is proportional to the kinetic energy or the velocity squared. Using this procedure we calculated the rock fall end points, spatial density and kinetic energy along the falling paths for all source points identified by DTP. In this way the 2.5D modeling approach can provide more realistic results than 2D modeling. Finally, the dispersion analysis was refined specifically for those blocks that, after runout simulation, were capable of reaching the railroad line. Rock fall hazard was then assessed by combining the maps of density, kinetic energy and geomorphology.

4. Results

4.1. Rock mass classification and stability assessment

Fieldwork combined with information in the literature and interpretations of photographs resulted in the new geological and geomorphological map shown in Fig. 2, and the reconstruction of the structural setting. Two main discontinuity systems characterize the rock mass: K1 [sub-system K1a (dip direction/dip recorded as 222/81) and sub-system K1b (38/74)] and K3 (301/53) (Table 2). A third system, K2 (146/34), was associated with the local foliation of the green schist facies.

Data related to joints and geo-engineering characteristics (Table 2) were used to calculate the *RMR* and *SMR* parameters (Tables 3 and 4). According to the *SMR* values, the rocky mass was classified as "fair" (Class III) with "probable block generation and instability along plans or wedges that need systematic slope stabilization". This result was confirmed by the *Q* System with a value $Q=4$, corresponding to Fair–Poor rock mass quality (Classes V–VI). Classification of the rock mass was based on field measurements (578 entries). A further 697 entries from DTP improved the characterization of joints, with data on attitude, persistence and spacing.

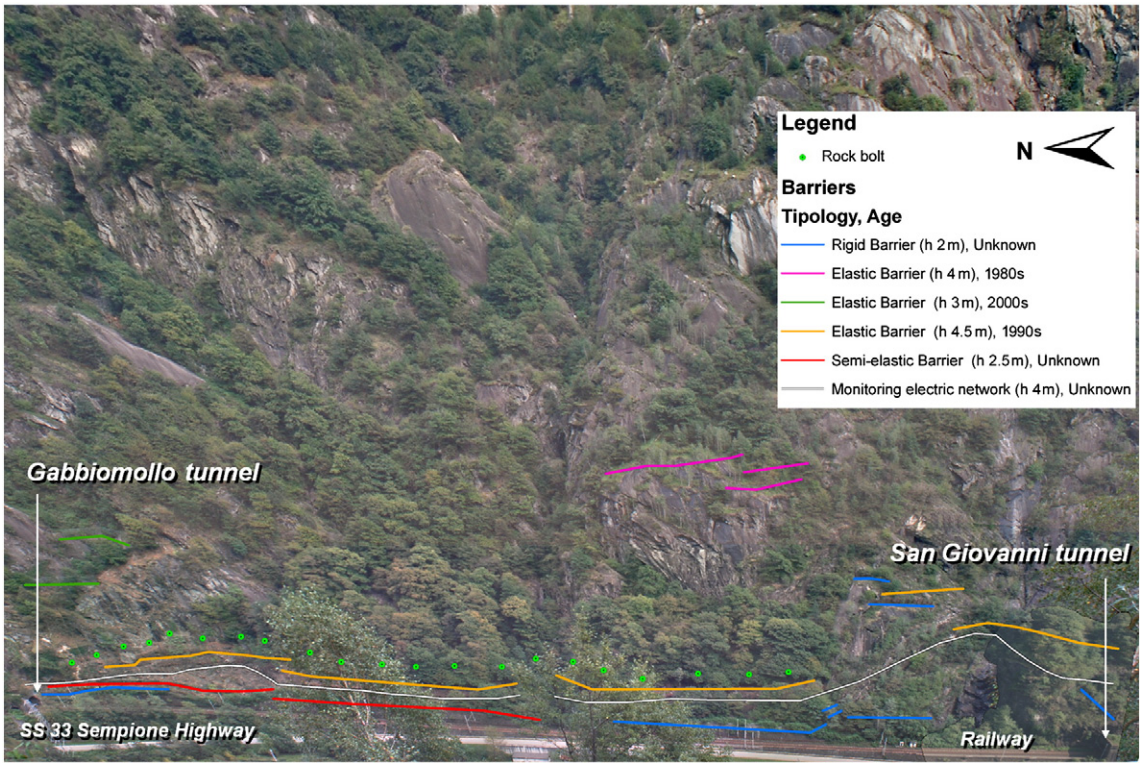

Fig. 6. Data collection and mapping of existing protection measures.

Table 2
Geo-engineering data.

SET	K1a	K1b	K2	K3
ATTITUDE (dip dir/dip — degrees)	222/81	38/74	146/34	301/53
APERTURE (mm)	54	50	54	54
PERSISTENCE (m)	2.5	2.9	2.3	1.8
SPACING (cm)	42	19	44	71
WEATHERING	Moderately altered	Moderately altered	Moderately altered	Moderately altered
FILLING	Absent-soft	Absent-soft	Absent-soft	Absent-soft
ROUGHNESS	Rough	Rough	Rough	Very rough
WATER	Dry	Dry	Dry	Dry
JCS (MPa)	64.6	64.21	59.04	61.03
JRC	9	9	9	11

Measures from DTP, with accuracy already assessed relative to TLS as shown in Fig. 4, were compared with fieldwork data by means of a density analysis of attitudes in stereographic projection (Fig. 7). Similarities between the K1b and K2 systems are evident. The K1a and K3 systems show good correspondence (Table 5), but the photogrammetric data has greater dispersion. This is because the geo-engineering survey was carried out in reachable outcrops at the bottom of the slope, whereas DTP photointerpreted joints refer to the whole versant 35 ha wide; the larger the area under study, the more the attitude of joints may vary. Nevertheless, the mean attitude derived from the two methods correspond well, with data variability always less than 10° (Table 5). DTP successfully stereorestituted several tens of rocky blocks and wedges, with sizes ranging from 0.16 to 210.50 m^3 and a mean value of 12 m^3 and a mode smaller than 1 m^3.

The stability kinematic analysis indicated a greater probability of planar sliding along the K1a system and along the K1a and K3 intersection lines. The static analysis revealed that 18.8% of potentially unstable blocks have a critical SF, with the percentage increasing to 29.9% during the dynamic analysis in anhydrous conditions (Table 6). The dynamic analysis found that water saturation and applied seismic acceleration can influence the stability of almost all blocks (Table 6). With regard to stability, Fig. 8 shows the geometrical relation between the slope and joint systems; the K3 system daylights into the slope, and K1a is sub-parallel to the slope or near vertical. In the dynamic analysis, it is relevant that this geo-structural setting favors water circulation in the fractures and beneath rock blocks resting on inclined planes, thereby inducing instability.

4.2. Rock fall modeling and hazard assessment

As an accurate slope model may improve the rock fall simulation, the differences in elevation between the DTM and the DSM were computed.

Table 3
Rock mass quality classification according to *RMR*. *A*1 = strength of intact rock material; *A*2 = rock quality designation (*RQD*; Deere et al., 1967); *A*3 = joint spacing; *A*4 = joint condition; *V*1 = joint persistence; *V*2 = joint aperture; *V*3 = joint roughness; *V*4 = joint weathering; *V*5 = joint filling; *A*5 = groundwater in joint; *RMRb* = basic *RMR*.

Parameter	Set			
	K1a	K1b	K2	K3
*A*1	5	5	5	5
*A*2	15	15	15	15
*A*3	9	8	9	12
*V*1 *Persistence*	4	4	4	4
*V*2 *Aperture*	0	0	0	0
*V*3 *Roughness*	5	5	5	6
*V*4 *Weathering*	3	4	4	4
*V*5 *Filling*	2	2	2	2
*A*4	14	15	15	16
*A*5	15	15	15	15
RMRb	58	58	59	63

Table 4
Rock slope classification according to *SMR*. *F*1 depends on the parallelism between discontinuity dip direction and slope dip. *F*2 depends on the discontinuity dip, in the case of planar failure, and the plunge of the intersection line in wedge failure. *F*3 depends on the relationship between slope and discontinuity dips, in the case of planar failure, or the plunge of the intersection line in wedge failure. *F*4 is a correction factor that depends on the excavation method used.

Set	*F*1	*F*2	*F*3	*F*4	*SMR*
K1a	0.4	1	−50	15	53
K1b	0.15	1	−50	15	64
K2	0.15	0.85	−60	15	66
K3	0.4	1	−60	15	54

On the one hand the accuracy of the DTM is related to the source data, and in particular the scale of the topographic map used (1:10,000), the accuracy of contour lines (3.5 m; Kolbl, 2001) and the smooth shape of contours, which resulted from stereorestitution in mountain and vegetated areas from 1:37,500 scale aerial photographs taken in 1991. On the other hand the DSM was produced from a point cloud with a spatial resolution of 5 cm for a 500 m distance. The differences in elevation between the DTM and the DSM were assessed showing a normal distribution of results with an average value of 1.7 m and a standard deviation of 17.1 m. The DSM was then used to calculate the block trajectories along the morphological profile, together with their kinetic energy and cover distance. The accuracy of rock fall paths relative to the line of steepest descent was checked by GIS spatial analyses. Fig. 9a shows the simulation results of 3D trajectories for the total number of blocks that have a critical *SF* value based on the highest percentage of water saturation and seismic coefficient. This choice is based on a precautionary approach hypothesizing the worst rock fall scenario. Fig. 9b shows the distribution of the simulated rock fall transit density, indicating good spatial correspondence with trajectories down the path of the steepest descent. The rock fall transit density has a wide dispersion about the inferred line of the steepest descent that was considered in the hazard mapping as discussed later. When modeling the runout, however, the choice of studying the fall paths along the steepest gradient, leads to consider the maximum kinetic energy and therefore the most hazardous rock fall paths.

Based on the type of protective barriers and their state of conservation, two different runout scenarios were simulated. The first scenario considered the maximum impact energy that the barriers can support (900 kJ), and the second scenario reduced this figure by 30% (to 630 kJ). In the first simulation, 12% of blocks reached the railway line and 10% of blocks were stopped by the protective barriers; the remaining masses ended their fall in vegetated areas, where the slope steepness decreases, or above the railway tunnels. In the second scenario the percentage of blocks stopped by the barriers was 7%, and 15% of blocks ended their fall on the railway (Fig. 9c). For the latter case, a newly refined dispersion map was created (Fig. 9d).

From the spatial overlay involving rock fall transit density, kinetic energy (Fig. 10a) and geomorphology (Fig. 2), a rock fall hazard map was generated (Fig. 10b). This displayed the areas of very high risk, which coincided with historical evidences and contained the main trajectories of rock falls. This zoning criterion, together with the kinetic energy of falling blocks, can be used to recommend the protection work that should be carried out by local authorities in specific areas.

Table 5
Mean values of joint systems attitude from the geo-engineering survey and DTP.

System	Engineering geological (degrees)	DTP (degrees)
K1a	222/81	228/75
K1b	38/74	42/77
K2	146/34	142/36
K3	301/53	305/64

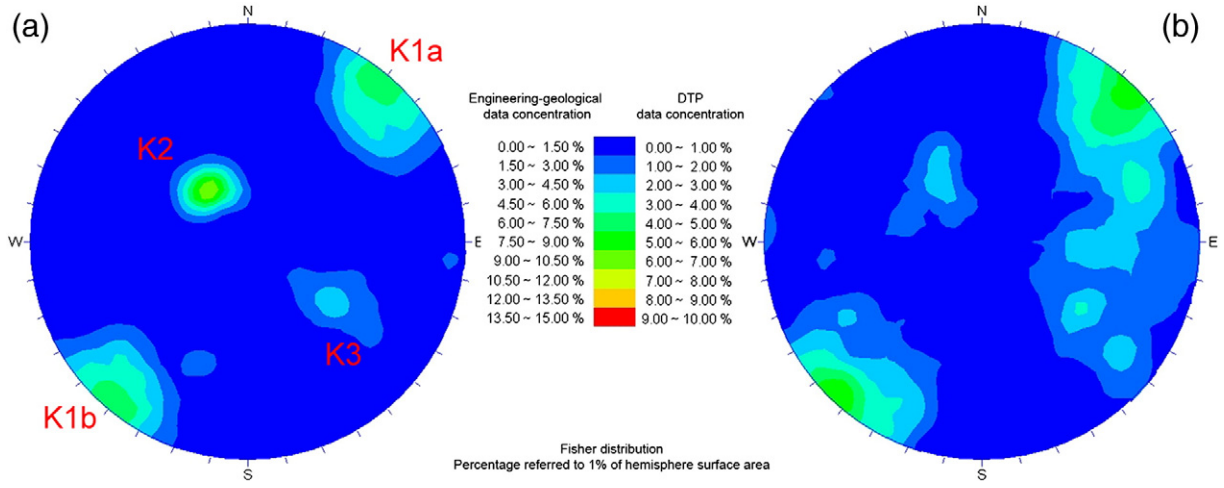

Fig. 7. Contour plots of joint systems from geo-engineering survey (a) and DTP (b). Data is presented using stereographic projection through the Schmidt equal-area method.

5. Discussion

Remote sensing technologies, such as DTP and TLS, can be used to study rocky slope stability and runout, overcoming problems such as inaccessibility of outcrops and complex slope morphology. DTP is fairly complicated and time-consuming, whereas TLS has proved to be a rapid and accurate way to model the morphology. In recent years, laser scanning has also been proposed as alternative to DTP for modeling the slope and attitude of discontinuities and for studying rock slope stability (Olariu et al., 2008; Runqiu and Xiujun, 2008; Mah et al., 2011). In the present work, the distance from the TLS station to the slope, and the consequent low density of points in the cloud, together with the importance of understanding the rock mass geo-structure, led us to use TLS only for building the DSM and slope profiles. DTP was used for a detailed geometrical study of joints and blocks. Furthermore, large vegetated areas masked the rocky outcrops, creating shadows in TLS data which are conditional on fixed stations and tied instrumental lights of sight. These deficiencies were accentuated because the percentage of bare rock surface in the total study area is 48%, which corresponds to 17 ha. TLS deficiencies in the automatic building of DSM and photointerpretation of geological and geomorphological features were consequently overridden by DTP, using very close shots orthogonal to the slope that allowed an easy stereorestitution. Recent studies (Haneberg, 2005; Tonon and Kottenstette, 2006; Sturzenegger and Stead, 2009) have demonstrated that terrestrial laser scanning and close-range terrestrial digital photogrammetry together represent a new and effective technology for characterizing rock masses. In this sense, the use of these technologies was best considered as supplementary rather than an alternative. We also have successfully used laser scanning, together with DTP, to improve the accuracy of 3D modeling, the efficiency of stability analysis, and the reliability of rock fall simulation (Francioni et al., 2010; Salvini et al., 2011).

Table 6
Percentages of blocks with critical SF, varying the water saturation in joints and applying the local seismic acceleration (*sc* = seismic coefficient).

% saturation	*sc* = 0	*sc* = 0.056
0	18.8%	29.9%
20	36.8%	50.4%
50	60.7%	65.8%
80	79.5%	84.6%
100	88.9%	91.5%
Stable	11.1%	8.5%

Deterministic geometrical data, derived from the application of TLS and DTP, were used to full advantage in studying slope stability by conventional methods of limit equilibrium. This method is simple and widely used, but it is limited to easy problems such as regular slope geometry and basic loading conditions. Many difficulties in studying rock slope stability are due to complexities related to geometry, material anisotropy, non-linear behavior, in situ stresses and the presence of several coupled processes (Stead et al., 2001); the method does not take into account the presence of rock bridges, vegetation and exogenous agents in material degradation. In such cases, as in the present study, conventional methods of stability analysis may be useful in reconstructing the trigger mechanism that initiates a failure event, but they are ineffective for modeling its evolution and impact

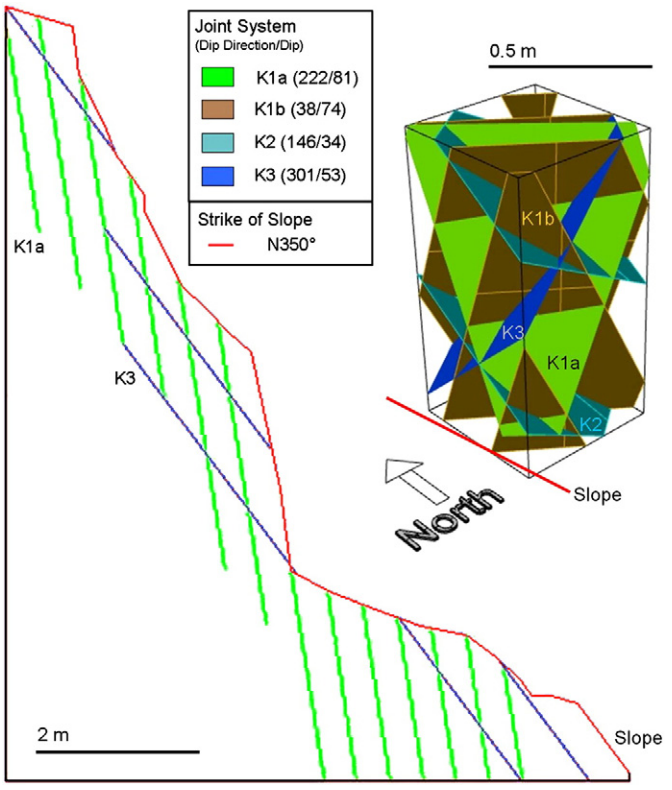

Fig. 8. Bi-dimensional scale modeling of the most probable sliding systems, and three-dimensional representation of the facing of all discontinuities on the slope.

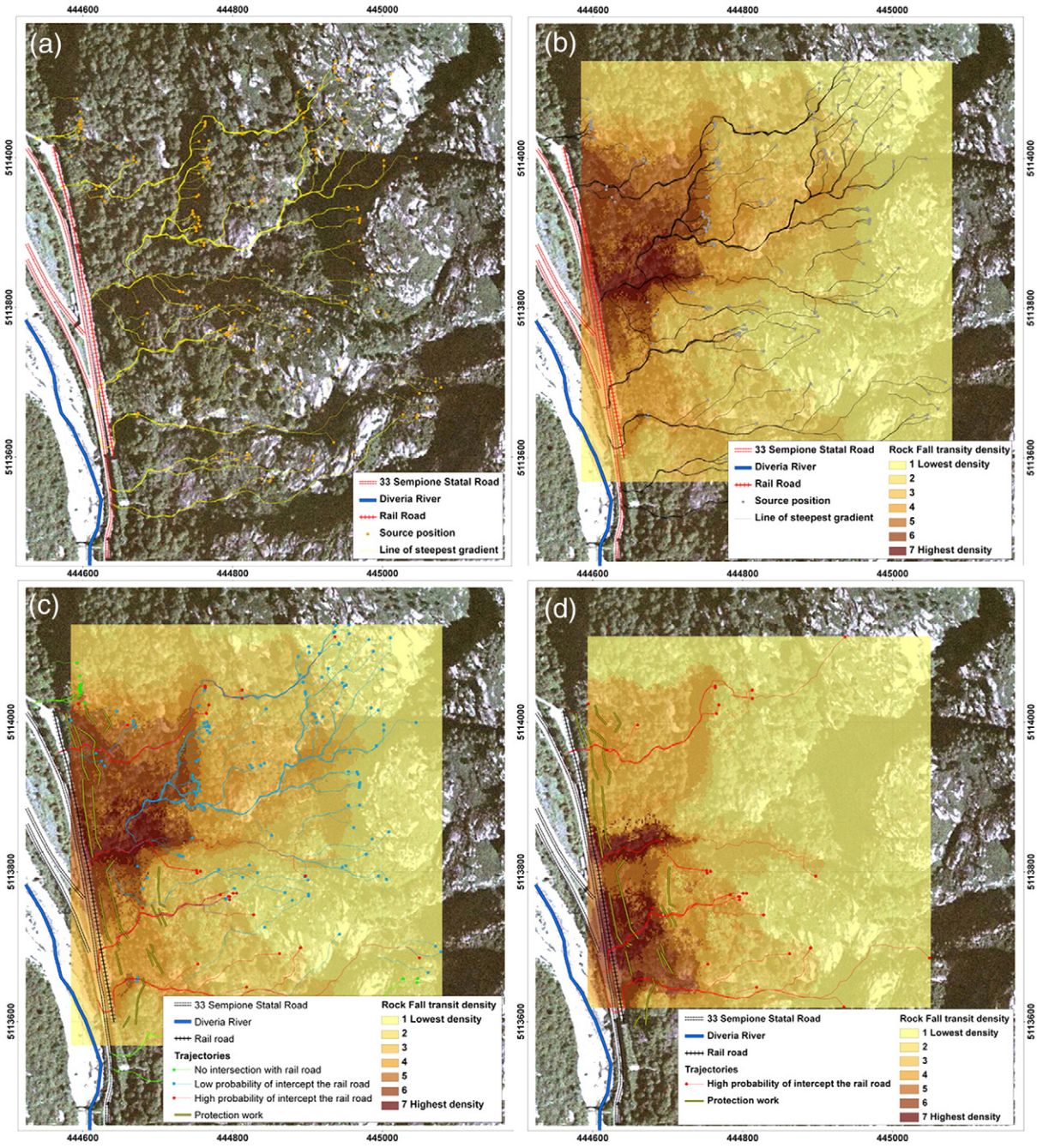

Fig. 9. Rock fall modeling. (a) Lines of steepest descent and source positions. (b) Rock fall transit density. (c) Rock fall transit density with block trajectories. d) Rock fall transit density for blocks reaching the railroad line.

on overall stability. Configurations used in analyzing the stability of the whole slope can be represented using a finite number of individual components. Such systems, termed "discrete", relate to rock masses controlled by discontinuity behavior (Jing and Stephansson, 2007), and take advantage of the deterministic approach to geometric information. We are currently working with the Itasca™ UDEC code in order to study the interactions among distinct blocks subjected to external loads and dependent on time and on physical–mechanical characteristics of the material involved (Cundall and Hart, 1992). Limiting factors in this work are related to the determination of some geo-engineering parameters, such as the friction angle, which was evaluated directly from fieldwork using empirical methodologies, and from a back analysis, since data from the laboratory or in situ tests was not available.

Rock fall modeling and its spatial distribution require the input data to be as accurate as possible (Lan et al., 2007, 2010; Monnet et al., 2010). This is because high-resolution data includes slope micro-reliefs and artificial features such as railway protection measures. As far as runout is concerned, 2D simulation has a major limitation regarding the subjective creation of the rock fall profile, and lacks the modeling of the lateral trajectory dispersion. Lateral dispersion greatly influences the planning of effective safety measures and assessment of rock fall hazard. We sought to improve the accuracy of the analysis by verifying the spatial frequency of falling blocks using the "cone-method" employed by other authors to assess rock fall hazard (Aksoy and Ercanoglu, 2006; Ghazipour et al., 2008; Jaboyedoff and Labiouse, 2011). Softwares for 3D modeling, such as Rock fall Analyst (Lan et al., 2007), Stone (Guzzetti et al., 2002) and Pir3D (Cottaz

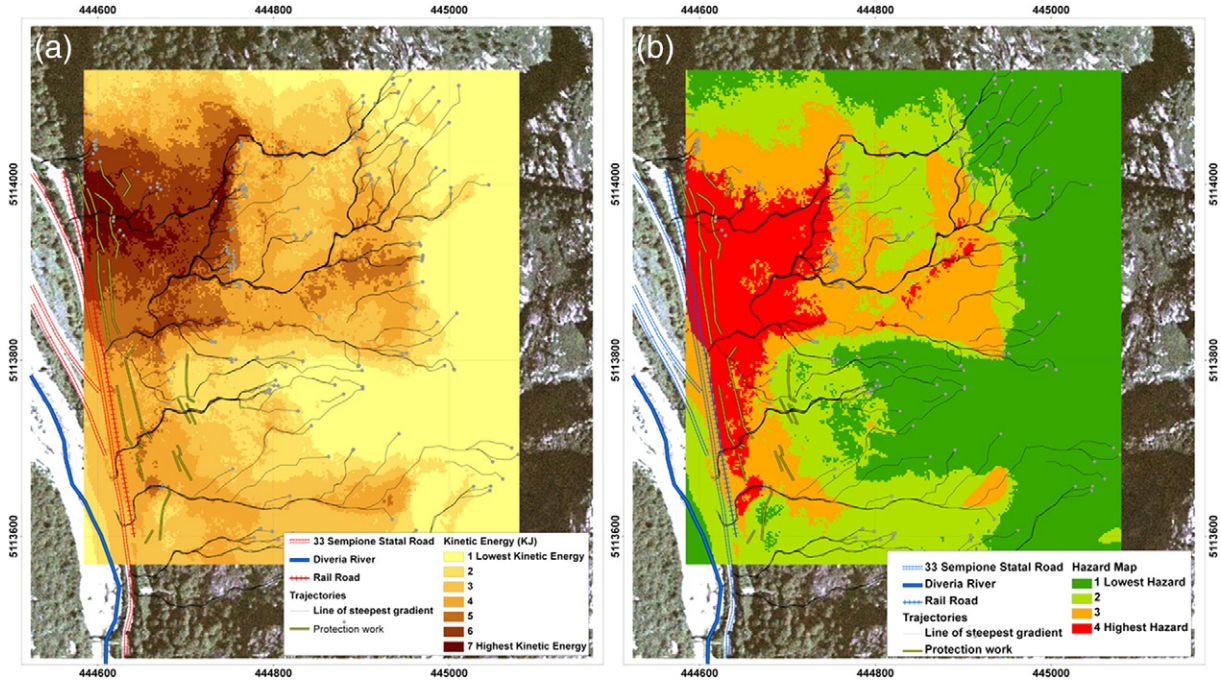

Fig. 10. Hazard assessment. (a) Rock fall kinetic energy. (b) Hazard map.

and Faure, 2008) consider the lateral dispersion of falling blocks, but have their limitations; for instance, they do not consider rock shape or fragmentation, since they use a "lumped mass" approach. Without considering the fragmentation of falling rocks, the kinetic energy of the rock mass is overestimated. Based on the 'rigorous' approach (Labiouse, 2007), we sought to overcome this limitation by statistically calibrating the coefficients of normal and tangential restitution, based on the size of collapsed blocks.

We successfully verified that the protective barriers already installed are placed correctly in the most hazardous areas, along the most probable trajectories of runout. A particular issue concerns the typology (elastic, semi-elastic and rigid), the geometry (height and size) and the state of conservation of barriers. Their age ranges from 10 to 25 years, so that their reliability is not guaranteed, even in an alpine environment characterized by low corrosiveness. As their efficacy against falling wedges depends on these parameters, and additional studies on the state of conservation have not been carried out until now, we decided to model the runout utilizing both reference and reduced values of their maximum impact energy.

6. Conclusions

In the present research, DTP and TLS provided powerful modeling and analytical tools for studying the stability of rocky slopes and rock fall hazard. The study area is characterized by steep slopes where several rock falls have been generated from vertical rock escarpments over the years. The main joint systems, traced to the late Alpine subduction phases, were surveyed during fieldwork and confirmed by DTP. The presence of several unstable blocks along the slope was highlighted by the geo-structural study. At the same time, geo-engineering analyses showed the fair quality of rock mass with associated planar or wedge failures, which represent a high geomorphologic risk for the railway located at the foot of the hill. Our stability analysis shows that hydraulic and seismic parameters strongly affect slope stability. The input data refer to a theoretical earthquake expected in the study area, and to the percentage of joint saturation modeled from statistical analysis of rainfall. Nevertheless, it must be underlined that the highest values of input data for the dynamic analysis are difficult to occur. The results of our rock fall analysis well agree with historical information and geomorphologic mapping. The distribution of rock fall frequency along the versant, and the location of high probabilities of rock fall occurrence are realistic.

There was a high hazard level at the northern and central parts of the railroad line, as evidenced by a fan of thick debris deposits. The risk at the tunnel openings is higher because the vertical escarpments directly overhang the railway tracks and, although there are artificial barriers, the protective measures are sometimes inadequate. Our results are useful for planning additional protection work (either active or passive, on the slope or directly close to the railway), and we propose that a displacement monitoring system could be set up via remote sensing (terrestrial SAR interferometry), and traditional (crack meters and extensometers) and topographic techniques (automated total station and GPS networks).

Acknowledgments

The authors wish to acknowledge the support by RFI (Rete Ferroviaria Italiana), ITALFERR (Società di Ingegneria delle Ferrovie dello Stato) and SGI (Studio Geotecnico Italiano).

Appendix A. Supplementary data

Supplementary data to this article can be found online at http://dx.doi.org/10.1016/j.geomorph.2012.12.020.

References

Abellán, A., Vilaplana, J.M., Martinez, J., 2006. Application of a long-range Terrestrial Laser Scanner to a detailed rock fall study at Vall de Núria (Eastern Pyrenees, Spain). Engineering Geology 88, 136–148.

Acosta, E., Agliardi, F., Crosta, G.B., Rìos Aragùes, S., 2003. Regional rock fall hazard assessment in the Benasque Valley (Central Pyrenees) using a 3D numerical approach. Mediterranean Storms. Proceedings of the 4th EGS Plinius Conference. Mallorca, Spain.

Aksoy, H., Ercanoglu, M., 2006. Determination of the rockfall source in an urban settlement area by using a rule-based fuzzy evaluation. Natural Hazards and Earth System 6, 941–954.

Argand, E., 1911. Les nappes de recouvrement des Alpes Pennines et leurs prolongements structuraux. Matière Carte Géologique Suisse, 31 (26 pp.).

Armesto, J., Ordonez, C., Alejano, L., Arias, P., 2009. Terrestrial laser scanning used to determine the geometry of a granite boulder for stability analysis purposes. Geomorphology 106, 271–277.
ARPA Regione Piemonte (Agenzia Regionale per la Protezione Ambientale), 2008. Banca Dati Geologica alla scala 1:100,000. http://gisweb.arpa.piemonte.it/arpagis/index.htm (access date 15 October 2009).
Barton, N.R., 1973. Review of a new shear strength criterion for rock joints. Engineering Geology 7, 287–332.
Barton, N.R., Lien, R., Lundle, J., 1974. Engineering classification of rock masses for the design of tunnel support. Rock Mechanics 6, 189–239.
Barton, N.R., Bandis, S.C., 1990. Review of predictive capabilities of JRC–JCS model in engineering practice. Proceeding of International Symposium on Rock Joints. Leon, Norway, pp. 603–610.
Besl, P.J., McKay, N.D., 1992. A method for registration of 3-D shapes. IEEE Transactions on Pattern Analysis and Machine Intelligence 14 (2), 239–256.
Bieniawski, Z., 1989. Engineering Rock Masses Classification. John Wiley and Sons Inc., New York (272 pp.).
Bigioggero, B., Boriani, A., Giobbi Mancini, E., 1977. Microstructure and mineralogy of an orthogneiss (Antigorio Gneiss — Lepontine Alps). Rendiconti Società Italiana di Mineralogia e Petrologia 33, 99–108.
Boriani, A., 2000. The geo-petrological setting of the Verbano–Ossola domain in the frame of the Alps. Proceeding of International Congress Quarry-Laboratory-Monument. Pavia, Italy, 1, pp. 1–14.
CNR (Consiglio Nazionale delle Ricerche), 1990. Structural Model of Italy 1:500,000. Sheets 1 and 2 (Alps). SELCA, Firenze.
Copons, R., Vilaplana, J.M., 2008. Rock fall susceptibility zoning at a large scale: from geomorphological inventory to preliminary land use planning. Engineering Geology 102, 142–151.
Cottaz, Y., Faure, R.M., 2008. Pir3D, an easy to use three dimensional block fall simulator. Landslides and Engineered Slopes. From the past to the future. Proceedings of the 10th International Symposium on Landslides and Engineered Slopes. Xi'an, China, p. 28.
Crosta, G.B., Agliardi, F., 2003. A methodology for physically-based rock fall hazard assessment. Natural Hazards and Earth System 3, 407–422.
Crosta, G.B., Agliardi, F., 2004. Parametric evaluation of 3D dispersion of rock fall trajectories. Natural Hazards and Earth System 4, 583–598.
Cundall, P.A., Hart, R.D., 1992. Numerical modeling of discontinua. Engineering Computers 9 (2), 101–113.
Deere, D.U., Miller, R.P., 1966. Engineering classification and index properties for intact rock. Technical Report AFNL-TR-65-116.Air Force Weapons Laboratory, New Mexico (277 pp.).
Deere, D.U., Hendron, A.J., Patton, F.D., Cording, E.J., 1967. Design of Surface and Near Surface Constructon in Rock. In: Fairhurst, C. (Ed.), Failure and Breakage of Rock. Proceedings of the 8th Symposium on Rock Mechanics. Society of Mining Engineers of American Institute of Mining Engineers, New York, pp. 237–302.
Di Crescenzo, G., Santo, A., 2007. High-resolution mapping of rock fall instability through the integration of photogrammetric, geomorphological and engineering-geological surveys. Quaternary International 171–172, 118–130.
Dorren, L.K.A., 2003. A review of rock fall mechanics and modelling approaches. Progress in Physical Geography 27, 69–87.
Evans, S.G., Hungr, O., 1993. The assessment of rock fall hazard at the base of talus slopes. Canadian Geotechnical Journal 30, 620–636.
Evans, S.G., Savigny, K.W., 1994. Landslides in the Vancouver–Fraser Valley–Whistler region. Geology and geological hazards of the Vancouver Region, Southwestern British Columbia: Geological Survey of Canada Bulletin, 481, pp. 251–286.
Fekete, S., Diederichs, M., Lato, M., 2010. Geotechnical and operational applications for 3-dimen. laser scanning in drill and blast tunnels. Tunnelling and Underground Space Technology 25, 614–628.
Feng, Q.H., Röshoff, K., 2004a. In-situ mapping and documentation of rock faces using full-coverage 3D laser scanning techniques. International Journal of Rock Mechanics and Mining 41, 139–144.
Feng, Q.H., Röshoff, K., 2004b. In-situ mapping and documentation of rock faces using full-coverage 3D laser scanning techniques [conference abstract]. International Journal of Rock Mechanics and Mining 41, 379.
Ferrero, A.M., Forlani, G., Rondella, R., Voyat, H.I., 2009. Advanced geostructural survey methods applied to rock mass characterization. Rock Mechanics and Rock Engineering 42 (4), 631–665.
Firpo, G., Salvini, R., Francioni, M., Ranjith, P.G., 2011. Use of Digital Terrestrial Photogrammetry in rocky slope stability analysis by Distinct Elements Numerical Methods. International Journal of Rock Mechanics and Mining 48 (7), 1045–1054.
Francioni, M., Salvini, R., Riccucci, S., Machetti, E., 2010. Tecnologie geomatiche per l'analisi di stabilità dei fronti rocciosi tramite modellazione numerica ad elementi distinti. Proceedings of the 14° Conferenza Nazionale ASITA. Brescia, Italy, II, pp. 1025–1030.
GeoStru, 2008. GeoStru PS Software. http://www.geostru.com/geoapp/parametrisismici.aspx (access date 11 January 2010).
Ghazipour, N., Uromeihy, A., Entezam, I., Ansari, F., Pirouz, M., 2008. The use of cone-fall theory for evaluation of rock-fall hazard along the Chaloos-Road (Pol-e-Zanguleh–Marzan-Abad). Geosciences 17, 160–169.
Glenn, N.F., Streutker, D.R., Chadwick, D.J., Thackray, G.D., Dorsch, S.J., 2006. Analysis of LiDAR-derived topographic information for characterizing and differentiating landslide morphology and activity. Geomorphology 73, 131–148.
Guzzetti, F., Crosta, G., Detti, R., Agliardi, F., 2002. STONE: a computer program for the three-dimensional simulation of rock falls. Computer and Geoscience 28, 1079–1093.
Haarbrink, R.B., Eisenbeiss, H., 2008. Accurate DSM production from unmanned helicopter systems. International Archives of Photogrammetry, Remote Sensing and Spatial Information Sciences, XXXVII/B1. PRC, Beijing, pp. 159–164.
Haneberg, W.C., 2005. 3D digital rock mass characterization using high-resolution photogrammetric or laser scanner point clouds. Abstracts programs. Geological Society of America 37 (7), 245.
Haneberg, W.C., 2008. Using close range terrestrial digital photogrammetry for 3-D rock slope modelling and discontinuity mapping in the United States. Bulletin of Engineering Geology and the Environment 67, 457–469.
Heim, A., 1932. Bergsturz und Menschenleben. Fretz und Wasmuth Verlag, Zurich (218 pp.).
Höhle, J., Höhle, M., 2009. Accuracy assessment of digital elevation models by means of robust statistical methods. ISPRS Journal of Photogrammetry and Remote Sensing 64, 398–406.
Hunziker, J.C., 1966. Zur Geologie und Geochimie des Gebietes zwischen Valle Antigorio (Novara) und Valle di Campo (Kt. Tessin). Schweizerische Mineralogische und Petrographische 46, 473–567.
Hutchinson, J.N., 1988. Morphological and geotechnical parameters of landslides in relation to geology and hydrogeology. Proceedings of the 5th International Symposium on Landslides. Lausanne, Switzerland, pp. 3–35.
Hutchinson, D.J., Diederichs, M.S., Carranza-Torres, C., Sherieff, C., Kjelland, N., Harrap, R., 2006. Landslide hazard management using geotechnical monitoring, virtual process models and decision support technology. Felsbau Rock and Soil Engineering 24 (3), 24–29.
Hyndman, D., Hyndman, D., 2008. Natural Hazards and Disasters, Second edition. Brooks Cole/Cengage Learning, Belmont CA, USA (555 pp.).
Jaboyedoff, M., Labiouse, V., 2003. Preliminary assessment of rockfall hazard based on GIS data. 10th International Congress on Rock Mechanics ISRM 2003, Technology Roadmap for Rock Mechanics. South African Institute of Mining and Metallurgy, Johannesburg, South Africa, pp. 575–578.
Jaboyedoff, M., Dudt, J.P., Labiouse, V., 2005. An attempt to refine rock fall hazard zoning based on the kinetic energy, frequency and fragmentation degree. Natural Hazards and Earth System Sciences 5, 621–632.
Jaboyedoff, M., Labiouse, V., 2011. Technical note: preliminary estimation of rockfall runout zones. Natural Hazards and Earth System Sciences 11, 819–828.
Jing, L., Stephansson, O., 2007. Fundamentals of Discrete Element Methods for Rock Engineering Theory and Applications. Elsevier Publishers, Oxford, UK (545 pp.).
Joos, M., 1969. Zur Geologie und Petrographie der Monte Giove-Gebirgsgruppe im östlichen Simplon-Gebiet (Novara-Italia). Schweizerische Mineralogische und Petrographische 49, 277–323.
Kaab, A., 2000. Photogrammetry for early recognition of high mountain hazards: new techniques and applications. Physics and Chemistry of the Earth B 25, 765–770.
Kolbl, O., 2001. Technical specification for the elaboration of Digital Elevation Model. Ecole Politecnique Federale de Lausanne, Department de Genie Rural. Report Version 4, pp. 26–32.
Labiouse, V., 2007. Prediction of rock fall trajectories. Mountain Risks, Workshop II: Single Hazard Analysis. Lausanne, Switzerland.
Lan, H., Derek Martin, C., Lim, C.H., 2007. Rock fall analyst: a GIS extension for three-dimensional and spatially distributed rock fall hazard modelling. Computers and Geosciences 33, 262–279.
Lan, H., Derek Martin, C., Zhou, C., Lim, C.H., 2010. Rock fall hazard analysis using LiDAR and spatial modelling. Geomorphology 118, 213–223.
Lim, C.H., Derek Martin, C., Herd, E.P.K., 2004. (CD-ROM) Proceedings of the 57th Canadian Geotechnical Conference. Quebec City, Canada, pp. 1–8.
Loye, A., Pedrazzini, A., Jaboyedoff, M., 2008. Regional potential rock fall mapping using LiDAR-based slope frequency distribution and conefall modelling. Geophysical Research Abstracts, 10. EGU General Assembly, Vienna, Austria (EGU2008-A-08546).
M. LL. PP. Ministero dei Lavori Pubblici, 1988. Norme tecniche riguardanti le indagini sui terreni e sulle rocce, la stabilità dei pendii naturali e delle scarpate, i criteri generali e le prescrizioni per la progettazione, l'esecuzione e il collaudo delle opere di sostegno delle terre e delle opere di fondazione. D.M. del 11.03.1988. Gazzetta Ufficiale della Repubblica Italiana (01.06.1988, 127 pp.).
M. LL. PP. Ministero dei Lavori Pubblici, 2008. NTC - Norme Tecniche per le Costruzioni. D.M. del 14/01/2008. Gazzetta Ufficiale della Repubblica Italiana, 04.02.2008, pp. 15–25 (and pp. 196–198).
Mah, J., Samson, C., McKinnon, S.D., 2011. 3D laser imaging for joint orientation analysis. International Journal of Rock Mechanics and Mining Science 48, 932–941.
Mantckelow, N., 1985. The Simplon line: a major displacement zone in the western Lepontine Alps. Eclogae Geologicae Helvetiae 78, 73–96.
Markland, J.T., 1972. A useful technique for estimating the stability of rock slopes when the rigid wedge sliding type of failure is expected. Imperial College Rock Mechanics Research Reprints, 19 (10 pp.).
Marquinez, J., Menéndez, R., Farias, P., JiméNez Sànchez, M., 2003. Predictive GIS-based model of rock fall activity in mountain cliffs. Natural Hazards 30, 341–360.
Matsuoka, N., Sakai, H., 1999. Rock fall activity from an alpine cliff during thawing periods. Geomorphology 28, 309–328.
Monnet, J.M., Clouet, N., Bourrier, F., Berger, F., 2010. Using geomatics and airborne laser scanning for rock fall risk zoning: a case study in the French Alps. Canadian Geomatics Conference and Symposium of Commission I (ISPRS). Calgary, Alberta, Canada.
Montgomery, D., Brandon, T., 2002. Topographic controls on erosion rates in tectonically active mountain ranges. Earth and Planetary Science Letters 201, 481–489.
Mosaad Allam, M., 1978. The estimation of fractures and slope stability of rock faces using analytical photogrammetry. Photogrammetria 34 (3), 89–99.
Ohnishi, Y., Nishiyama, S., Yano, T., Matsuyama, H., Amano, K., 2006. A study of the application of digital photogrammetry to slope monitoring systems. International Journal of Rock Mechanics and Mining 43, 756–766.

Olariu, M.I., Ferguson, J.F., Aiken, C.L.V., Xu, X., 2008. Outcrop fracture characterization using terrestrial laser scanners: deep-water Jackfork sandstone at Big Rock Quarry, Arkansas. Geosphere 4, 247–259.

Romana, M., 1985. New adjustment ratings for application of Bieniawski classification to slopes. Proceeding International Symposium on the role of rock mechanics ISRM, pp. 49–53.

Runqiu, H., Xiujun, D., 2008. Application of three-dimensional laser scanning and surveying in geological investigation of high rock slope. Journal of China University of Geosciences 19, 184–190.

Salvini, R., Fantozzi, P.L., Francioni, M., Riccucci, S., Bonciani, F., Mancini, S., 2011. Stability analysis of "Grotta delle Felci" Cliff (Capri Island, Italy): structural, engineering-geological, photogrammetric surveys and laser scanning. Bulletin of Engineering Geology and the Environment 70, 549–557.

Stead, D., Eberhardt, E., Coggan, J., Benko, B., 2001. Advanced numerical techniques in rock slope stability analysis — applications and limitations. UEF International Conference Landslides — Causes, Impacts and Countermeasures. Davos, Switzerland, pp. 615–624.

Sturzenegger, M., Stead, D., 2009. Close-range terrestrial digital photogrammetry and terrestrial laser scanning for discontinuity characterization on rock cuts. Engineering Geology 106, 163–182.

Takumi, N., Ryoji, W., Norihiko, W., Yuzo, O., 2000. Rock slope displace measurement by photogrammetry system. Proceedings of the 30th Symposium on Rock Mechanics, pp. 213–217.

Tonon, F., Kottenstette, J.T., 2006. Laser and photogrammetric methods for rock face characterization. Report on a Workshop held June 17–18, 2006. Golden, Colorado.

Toppe, R., 1987. Terrain models — a tool for natural hazard mapping. Proceedings of the Davos Symposium. Avalanche formation, movement and effects. IAHS Publication 162, 629–638.

Vallet, J., Skaloud, J., Kölbl, O., Merminod, B., 2000. Development of a helicopter based integrated system for avalanche and hazard management. International Archives of Photogrammetry and Remote Sensing 33 (B2), 565–572.

Van Knapen, B., Slob, S., 2006. Identification and characterisation of rock mass discontinuity sets using 3D laser scanning. Pre-proceedings of the 10th International Congress IAEG: Engineering Geology for Tomorrow's Cities. Nottingham, United Kingdom, 438, p. 11.

Whalley, W.B., 1984. Rock falls. In: Brunsden, D., Prior, D.B. (Eds.), Slope Instability. John Wiley and Sons, Chichester, pp. 217–256.

Wickens, E.H., Barton, N.R., 1971. The application of photogrammetry to the stability of excavated rock slopes. The Photogrammetric Record 7 (37), 46–54.

Yohei, U., Chikaosa, T., Keigo, K., Chunze, P., Shuichi, I., Zuixiong, L., 2007. Application of 3D laser scanning system to rock slope stability assessment in the Dunhuang Mogao. Proceedings of the 36th Symposium on Rock Mechanics. New York, USA, p. 27.

Yoon, W.S., Park, S.W., Shon, H., Park, H.J., Jeong, C.G., Han, B.H., 2006. Characterisation of rock slope failure within fault zone using laser scanning. Proceeding of the 41st U.S. Symposium on Rock Mechanics (USRMS). Golden, CO.

Zhang, Z., Kulatilake, P.H.S.W., 2003. A new stereo-analytical method for determination of removal blocks in discontinuous rock masses. International Journal for Numerical and Analytical Methods in Geomechanics 27, 791–811.